molecules

MDPI

Communication

The Homoleptic Curcumin–Copper Single Crystal (ML_2): A Long Awaited Breakthrough in the Field of Curcumin Metal Complexes

Antonino Arenaza-Corona [1,†], Marco A. Obregón-Mendoza [1,†], William Meza-Morales [2], María Teresa Ramírez-Apan [1], Antonio Nieto-Camacho [1], Rubén A. Toscano [1], Leidys L. Pérez-González [1], Rubén Sánchez-Obregón [1] and Raúl G. Enríquez [1,*]

[1] Instituto de Química, Universidad Nacional Autónoma de México, Ciudad de México 04510, Mexico; antoninoarenaza03@gmail.com (A.A.-C.); obregonmendoza@yahoo.com.mx (M.A.O.-M.); mtrapan@yahoo.com.mx (M.T.R.-A.); camanico2015@yahoo.com (A.N.-C.); toscano@unam.mx (R.A.T.); leidyslaura92@gmail.com (L.L.P.-G.); rubens@unam.mx (R.S.-O.)

[2] Department of Chemical Engineering, University of Puerto Rico-Mayaguez, Mayagüez, PR 00680, USA; willy_meza_morales@hotmail.com

* Correspondence: enriquezhabib@gmail.com; Tel.: +52-55562-24404

† These authors contributed equally to this work.

Abstract: The first single crystal structure of the homoleptic copper (II) ML_2 complex (M=Cu (II), L = curcumin) was obtained and its structure was elucidated by X-ray diffraction showing a square planar geometry, also confirmed by EPR. The supramolecular arrangement is supported by C-H···O interactions and the solvent (MeOH) plays an important role in stabilizing the crystal packing Crystallinity was additionally assessed by XRD patterns. The log P value of the complex (2.3 ± 0.15) was determined showing the improvement in water solubility. The cytotoxic activity of the complex against six cancer cell lines substantially surpasses that of curcumin itself, and it is particularly selective against leukemia (K562) and human glioblastoma (U251) cell lines, with similar antioxidant activity to BHT. This constitutes the first crystal structure of pristine curcumin complexed with a metal ion.

Keywords: curcumin–copper (II); single crystal; cytotoxicity; antioxidant

Citation: Arenaza-Corona, A.; Obregón-Mendoza, M.A.; Meza-Morales, W.; Ramírez-Apan, M.T.; Nieto-Camacho, A.; Toscano, R.A.; Pérez-González, L.L.; Sánchez-Obregón, R.; Enríquez, R.G. The Homoleptic Curcumin–Copper Single Crystal (ML_2): A Long Awaited Breakthrough in the Field of Curcumin Metal Complexes. *Molecules* **2023**, *28*, 6033. https://doi.org/10.3390/molecules28166033

Academic Editor: Miriam Rossi

Received: 28 June 2023
Revised: 1 August 2023
Accepted: 9 August 2023
Published: 12 August 2023

1. Introduction

Curcumin (diferuloylmethane, (1*E*,6*E*)-1,7-*bis*(4-hydroxy-3-methoxyphenyl)-1,6-heptadiene-3,5-dione) [1] is the major components of the Asian spice *Curcuma longa* [2] and has been extensively used in the biologic arena due to multiple purported effects such as antioxidant [3–5], anti-inflammatory [6,7], antiviral [8], antibacterial [9,10], antihypertensive, insulin sensitizer [11,12], cytotoxicity against cancer cell lines, and regulation of apoptosis [12–19]. However, this molecule has several disadvantages such as low solubility and therefore, poor bioavailability [20], poor stability, and fast metabolism [21,22], leading to hampered clinical applications [23].

Curcumin consists of an heptanoid chain with a conjugate β-keto-enol system two flanked by two aromatic rings (with an orto-methoxy-phenol system). Different research groups consider phenol groups responsible for their low stability [24] (due to quinoid conjugation type). Thus, the focus has been the synthesis of derivatives introducing alkyl (methoxycurcumin, ethoxycurcumin, butoxycurcumin) or acetyl (diacetylcurcumin, DAC) [25,26]. Additionally, to improve the solubility and overtake the bioavailability disadvantage, the formation of complexes with divalent (e.g., Zn^{+2}, Cu^{+2}, Mg^{+2}) [27–30] and more scarcely trivalent (e.g., Fe^{+3}, In^{+3}) metal ions [26,31] has been taken as the principal focus for the synthesis of metal complexes.

Historically, the synthesis of metallic complexes of curcumin began with several metal ions including physiologically relevant ones [27,32] (e.g., Zn, Cu, Mg, Mn, Fe, Se, Ni). However, structural characterizations so far are not conclusive from the solid-state point of view (i.e., Single crystal X-ray diffraction). Therefore, definitive proof of structural evidence of the coordination (ML, ML_2, or ML_3) between pristine curcumin and a metal ion was missing until now.

Then, a consistent line of reasoning found in the bibliography is that forming a molecular metal complex consisting of pristine curcumin with a metal ion leads to polymeric arrays due to free phenol groups [33,34]. Wang et al. derivatized the phenol groups using ethoxy or butoxy groups to obtain stable copper (II) ML_2 crystals [24]. From the biological point of view, Copper (II) is a necessary element to carry out several biological functions and is found widely distributed in connective tissues and blood vessels. A deficiency of this metal can cause different diseases such as anaemia [35], bone fragility [36], and increased susceptibility to infections [37]. In contrast, an excess (intoxication) of copper, is inconvenient and leads to Wilson's disease [38] and other neurological problems including Alzheimer's disease [39].

We have placed our efforts in the obtention of the curcumin–copper (II) complex, due to the important properties reported in the literature such as antioxidant, anti-inflammatory, antibacterial [40], antiviral, and antitumoral [41,42]. The chemical study of this complex has been carried out principally using spectroscopic (solution and solid-state) and spectrometric (ionization) techniques [43]. However, an electron density map derived from the X-ray single-crystal structure is now available. Currently, no reports describe the structural elucidation by single-crystal X-ray diffraction (Cambridge Crystallographic Data Center, 2023) between a curcumin molecule and a metal center in the ML_2 form.

In the obtention of the desired ML_2 complex of curcumin described herein (that we have named a "cherry on top"), several factors were considered and each one plays its role in turn. Thus, the chelation capability occurs preferentially at the β-diketone system rather than at the phenolic groups which render a stable six-membered ring system; a 2:1 strict ligand-metal stoichiometry. The copper acetate deprotonates the enol function of curcumin and produces a mild acidic media from the resulting acetic acid, which may help prevent the nucleophilic participation of phenol groups. Furthermore, the use of methanol as a solvent was found adequate after several attempts for crystallizing with other solvents.

2. Results

We are reporting the first molecular structure of a single crystal of copper and pristine curcumin coordinated in the ML_2 form. The synthesis of this complex was carried out as depicted in Scheme 1.

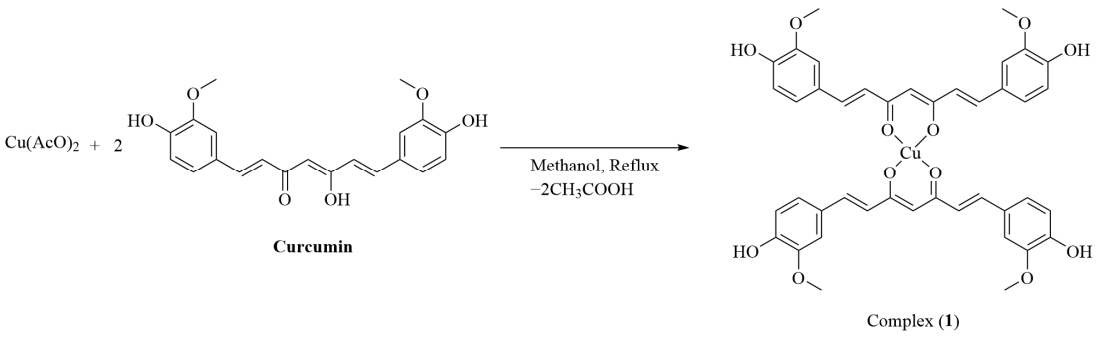

Scheme 1. Formation of ML_2 complex **1** from curcumin.

The solvated (MeOH) structure of curcumin–copper (II) (Complex **1**) crystallized in the triclinic system; space group P-1 (Z = 1) is shown in Figure 1 and the crystallographic data are shown in Supplementary Table S1. The curcumin (1E,6E)-1,7-bis(4-hydroxy-3-methoxyphenyl)-1,6-heptadiene-3,5-dione), also known with the common name difer-

uloylmethane, exhibits keto–enol tautomerism in solution (MeOH) adopting the enol tautomeric form (1E,4Z,6E)-5-hydroxy-1,7-bis(4-hydroxy-3-methoxyphenyl)hepta-1,4,6-trien-3-one (Scheme 1). Assuming this tautomeric form, curcumin still has four different rotation axes that can give rise to conformational isomers three of which have been determined by single crystal X-ray diffraction [44,45] (CSC refcodes: BINMEQ, BINMEQ12 and QUMDIN). The anti, s-cis, s-trans, anti-conformation (QUMDIN), where the term anti indicates the orientations of OCH_3 groups referred to the keto–enol moiety, was found for the ligand in its deprotonated form. Although the ligand molecule is nearly planar, the orientations of the phenyl groups are slightly twisted [C6-C7-C14-C15 = −2.1(3)° and C2-C1-C8-C9 = 8.4(4)°].

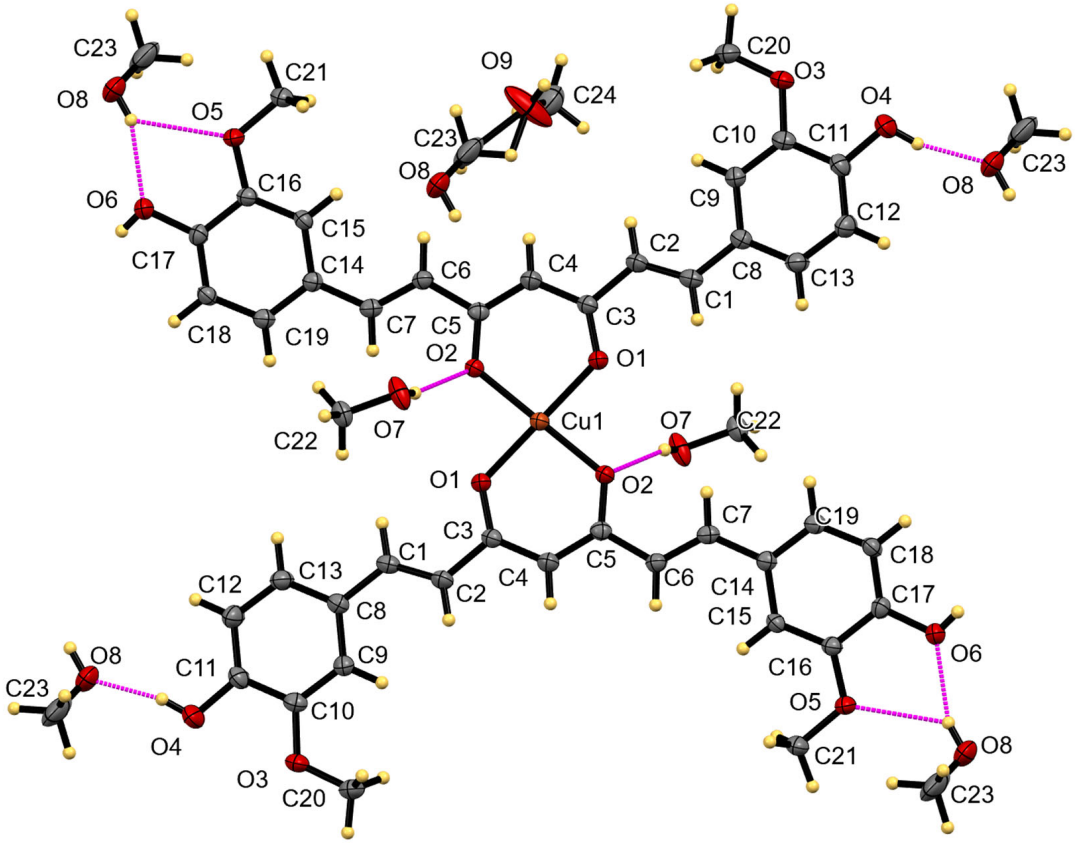

Figure 1. The molecular structure of the complex (**1**) shows the atom labelling, ellipsoids are represented at 50% of probability.

In the homoleptic complex (**1**), the copper atom resides on an inversion center with a nearly perfect square planar (τ_4 = 0.00) coordination. The four coordination sites are occupied by oxygen-donor atoms of the 1,6-heptadiene-3,5-dione moieties of curcumin. Thus, each curcumin acts as a bidentate chelate ligand Figure 1. The corresponding bond lengths are Cu-O1 = 1.9191(15) Å and Cu-O2 = 1.9192(14) Å, O1···O2 = 2.807(2) Å and O1···O2(−x, 1 − y, 1 − z) = 2.618(2) Å. The deviation of the mean planes of ligands to the coordination plane is 11.0°. Selected bond lengths are summarized in Table 1.

The metal complex (**1**) and pristine curcumin were screened against six cancer cell lines (see Supplementary Materials), and the metal complex was rendered more potent than curcumin itself, with selectivity against leukemia and glial cancer lines. The IC_{50} values were obtained for these two cell lines. The antioxidant tests were recorded in the lipid peroxidation inhibition model (TBARS), showing that the metal complex of curcumin acts against lipid oxidation.

Table 1. Selected bond lengths [Å] and angles [°] for complex (**1**).

Bond	Length	Bond	Length
Cu(1)-O(1)	1.9189(15)	C(3)-C(4)	1.407(3)
Cu(1)-O(2)	1.9191(14)	C(4)-C(5)	1.389(3)
O(1)-C(3)	1.280(2)	C(5)-C(6)	1.469(3)
O(2)-C(5)	1.292(2)	C(6)-C(7)	1.344(3)
C(1)-C(2)	1.340(3)	C(7)-C(14)	1.457(3)
C(1)-C(8)	1.458(3)		
C(2)-C(3)	1.466(3)		
Bonds	**Angle**	**Bonds**	**Angle**
O(1)-Cu(1)-O(2)#1	85.99(6)	C(1)-C(2)-C(3)-O(1)	−10.6(3)
O(1)-Cu(1)-O(2)	94.01(6)	C(1)-C(2)-C(3)-C(4)	169.6(2)
C(2)-C(1)-C(8)	126.4(2)	O(1)-C(3)-C(4)-C(5)	7.7(4)
C(1)-C(2)-C(3)	123.3(2)	C(2)-C(3)-C(4)-C(5)	−172.5(2)
O(1)-C(3)-C(4)	124.7(2)	Cu(1)-O(2)-C(5)-C(4)	−5.3(3)
O(1)-C(3)-C(2)	118.2(2)	Cu(1)-O(2)-C(5)-C(6)	175.8(1)
C(4)-C(3)-C(2)	117.1(2)	C(3)-C(4)-C(5)-O(2)	0.0(4)
C(5)-C(4)-C(3)	125.2(2)	C(3)-C(4)-C(5)-C(6)	178.9(2)
O(2)-C(5)-C(4)	124.3(2)	O(2)-C(5)-C(6)-C(7)	−9.4(3)
O(2)-C(5)-C(6)	117.0(2)	C(4)-C(5)-C(6)-C(7)	171.6(2)
C(4)-C(5)-C(6)	118.6(2)	C(5)-C(6)-C(7)-C(14)	175.3(2)
C(7)-C(6)-C(5)	122.2(2)	C(2)-C(1)-C(8)-C(9)	8.5(3)
C(6)-C(7)-C(14)	127.6(2)	C(6)-C(7)-C(14)-C(15)	−2.2(3)

Symmetry transformations are used to generate equivalent atoms: #1 −x, −y + 1, −z + 1.

3. Discussion

During the synthesis of the curcumin–copper complex (**1**), our main goal was the obtention of a single crystal of ML_2 type. Both solvent and raw materials were of high purity and a rigorous stoichiometry was used. Additionally, the filtrate and the solid precipitate were kept during the process for further workup. Further analysis (see ESI in Supplementary Materials, Figures S2–S4) showed that both solid and filtrated liquid contained curcuminoid fragments and metal.

However, the precipitate was found barely soluble even in large amounts of methanol and rendered an amorphous solid after full evaporation. We attribute this behavior to the possible polymeric nature of the product (m.p. = 290°). On the other hand, the filtrated mother liquor (containing metal-complex and a mixture of acetic acid/methanol) tends to spontaneously form crystals after slow evaporation and concomitant cooling, and these crystals redissolve readily in methanol at room temperature in an approximately 1:10 w/v ratio. In the latter case, the formation of a single crystal (suitable for X-ray diffraction) was successfully achieved by slow evaporation (see pictures in Figure S5).

EPR studies of crystals and amorphous solids (Figure 2 and Figure S6) show a typical four-line pattern of paramagnetic copper nuclei. The g∥, g⊥, A∥, and A⊥ values were obtained directly from the EPR spectra. The g∥ and g⊥ values of complex **1** were 2.290 and 2.059, resulting from unpaired electrons in the dx^2-y^2 molecular orbital [46]. The value of g∥ is <2.3, suggesting a covalent environment for this complex and the A∥ = 164 G supports the square-planar coordination of 4 equivalent oxygen atoms around the copper (II) ion. These parameters agree with those previously reported [28,47,48]. Furthermore, the CP/MAS spectrum of the ligand curcumin shows good resolution, contrasting with the very broad signals of the paramagnetic complex **1** (Figures S7 and S8).

Comparison of the IR-ATR spectra were carried out between (a) ligand and complex **1** and (b) amorphous material and monocrystals. The IR of curcumin (see Supplementary Materials Figure S9) shows signals at 3499 cm^{-1}, attributed to phenols (Ar-OH); stretching signals for the carbonyl group (C=O) at 1626 cm^{-1}, and the signal observed in 1601 cm^{-1} corresponds to vinyl groups (C=C). It has been reported that the intense IR signal at 1504 cm^{-1} is due to a mixture of vibrations of ν(C=O), δ(C-C=C), δ(C-C=O), and aromatics

at ν(C=C), ν(C=C-H) [49,50]. Complex **1** gives characteristic signals for the phenolic groups at 3443 cm^{-1}; the characteristic signals to the carbonyl group ν(C=O, 1619 cm^{-1}) and the vinyl groups (C=C, 1587 cm^{-1}), as well as the intense signal of 1491 cm^{-1}, are red-shifted with respect to the ligand due to Cu (II) coordination, as previously reported [49]. The IR spectrum of complex **1** shows a new signal at 478 cm^{-1} due to copper bonding to oxygen [8].

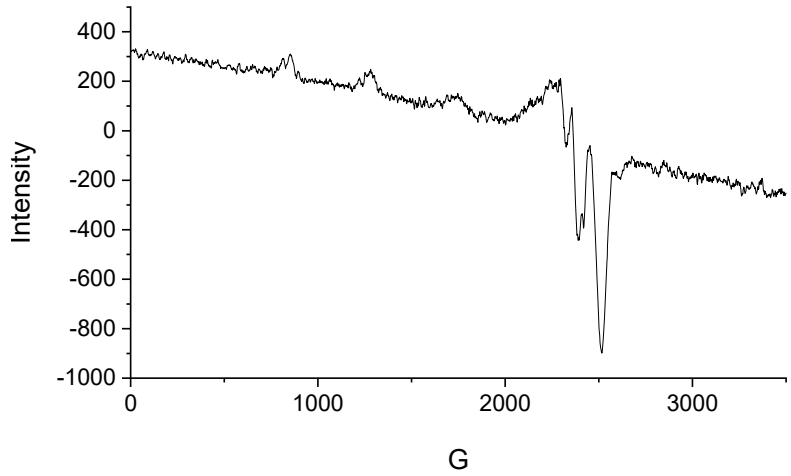

Figure 2. Electron Paramagnetic Resonance of the complex (**1**) compound at 77 K in methanol of brilliant brown crystalline (from mother liquor).

The IR spectra of both materials (amorphous and monocrystals, see Figures S10 and S11) show minimal but subtle differences, observed in the region of the phenol groups (amorphous 3441 cm^{-1} (broad signal) and crystals 3443 cm^{-1} (less broadened)). The additional signal at 3537 cm^{-1} for the crystalline complex is assigned to solvent molecules (methanol).

The UV-Vis spectrum of curcumin (1 μM) exhibits a maximum absorption peak at 420 nm in methanol (see Figures S9 and S10) and is attributed to $\pi \rightarrow \pi^*$ transitions [51]. The UV-Vis spectrum of complex **1** (1 μM) shows two characteristic absorption bands: 421 nm and 435 nm in methanol (see Figures S12 and S13) corresponding to the strong complexation between curcumin and copper (II) [51], these 2 absorption bands have also been attributed to charge transfer phenomena from curcumin to copper (II) [43,47].

The XRD pattern of complex **1** (single crystals) showed characteristic peaks (3.1, 3.5, 3.9, 4.3, 6.0, 7.1, 8.8, 12.1°), reflecting its crystallinity. However, the product that is retained in the filter shows a clear pattern of amorphous material, while the peaks found at 3.1 and 8.7° correspond to residual crystalline material retained (See the overlapping patterns in Figure 3 and individual patterns in Supplementary Materials Figures S14 and S15).

It is evident from PXRD patterns (Figure 3) that the material retained in the filter is almost completely amorphous with low crystallinity, while complex **1** displays good crystallinity. Despite the different temperatures between the simulated (130 K) and the experimental (298 K) patterns, enough correlation between them is observed, with noteworthy persistence of the 2,−1,2 diffraction peaks which can be associated with the supramolecular structure of complex **1** (See Figure S16 in Supplementary Materials including calculated pattern from obtained crystals).

In the crystal structure, the solvent molecules of methanol play key a role in the crystal architecture linking two neighboring complexes through two strong O4–H4···O8 and O8–H8···O6 hydrogen bonds generating a centrosymmetric cyclic dimer [graph set descriptor: $R_4^4(44)$] which extends infinitely. Furthermore, each 1D infinite chain interacts with two adjacent chains by non-classical hydrogen bonds (C21–H21A···O3 and C21–H21A···O4) forming a 2D sheet parallel to the (2,−1,2) crystallographic plane, Figure 4a. These sheets are interlaced by hydrogen bonds with the second methanol solvent molecule C22–O7 acting as a donor (O7–H7···O2) and acceptor (O6–H6···O7), gen-

erating another centrosymmetric cyclic dimer [graph set descriptor: $R_4^4(28)$] associated to an aromatic ⋯ metal chelate stacking Figure 4b.

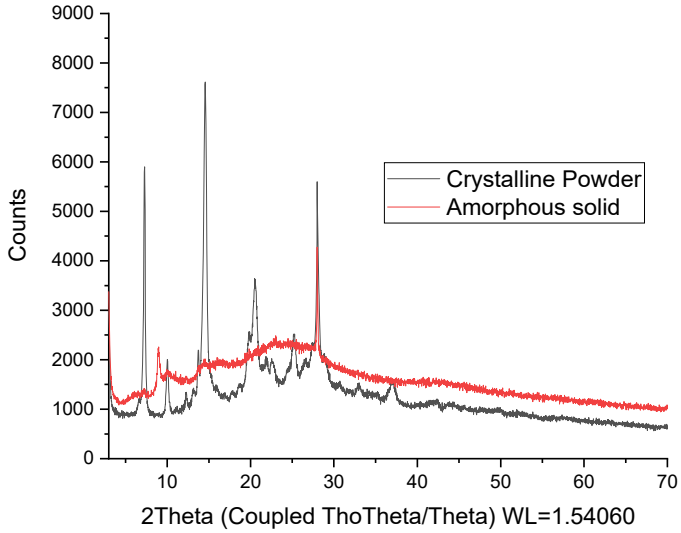

Figure 3. The experimental powder XRD patterns of two phases of complex **1**.

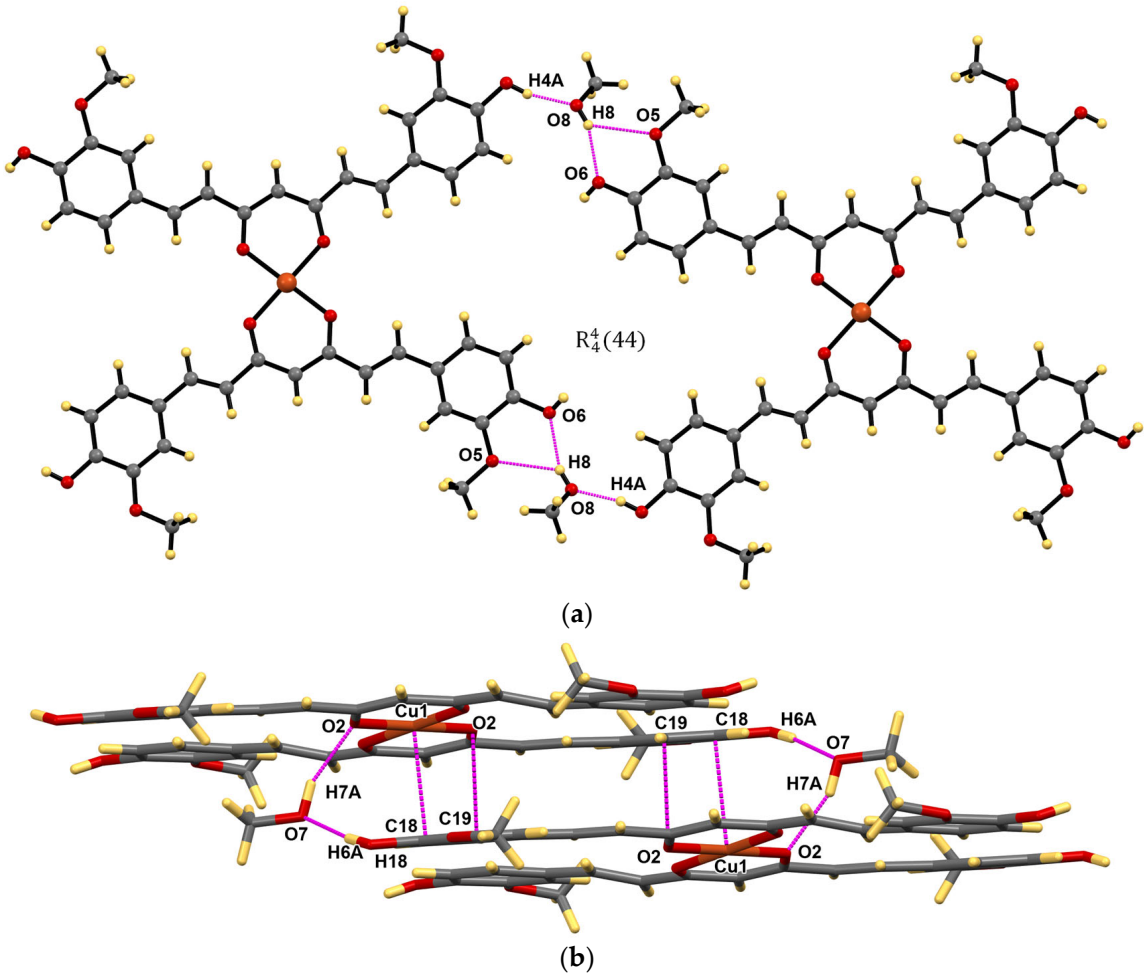

Figure 4. A supramolecular arrangement of the complex **1**; top view (**a**), side view (**b**).

The third methanol solvent molecule was found to be disordered around an inversion center and plays the role of void filling, although some contacts can be identified (Table 2).

Table 2. Hydrogen bonds for complex (**1**) [Å and °].

D-H···A	d(D-H)	d(H···A)	d(D···A)	<(DHA)
O(4)-H(4A)...O(8) #1	0.83	1.76	2.552(12)	160.9
O(4)-H(4A)...O(8B) #1	0.83	1.88	2.694(12)	166.7
O(6)-H(6A)...O(7) #2	0.76	2.02	2.767(12)	170.1
O(6)-H(6A)...O(7B) #2	0.76	1.82	2.574(10)	174.9
C(9)-H(9)...O(9B)	0.95	2.52	3.431(9)	161.0
C(18)-H(18)...O(7) #2	0.95	2.53	3.197(12)	127.4
C(20)-H(20A)...O(9B)	0.98	2.41	3.208(9)	138.4
C(21)-H(21A)...O(4) #3	0.98	2.64	3.580(3)	161.1
O(7)-H(7A)...O(2) #4	0.84	1.96	2.734(15)	153.2
O(8)-H(8)...O(5) #5	0.80	2.42	2.988(12)	129.3
O(8)-H(8)...O(6) #5	0.80	2.04	2.801(12)	159.7
C(23)-H(23C)...O(5) #6	0.98	2.46	3.129(10)	125.1
O(7B)-H(7B)...O(2) #4	0.84	1.99	2.786(14)	158.5
O(8B)-H(8B)...O(5) #5	0.84	2.39	3.070(11)	138.5
O(8B)-H(8B)...O(6) #5	0.84	2.11	2.861(11)	148.8
O(9)-H(9A)...O(4) #6	0.83	1.94	2.768(9)	179.3
C(24B)-H(24F)...O(4) #7	0.98	2.62	3.303(13)	126.9

Symmetry transformations used to generate equivalent atoms: #1 x + 1, y + 1, z; #2 x − 1, y − 1, z; #3 −x + 1, −y + 1, −z; #4 x + 1, y, z; #5 x, y + 1, z; #6 −x + 1, −y + 2, −z; #7 x, y − 1, z.

To obtain further information about close contacts in the crystal packing, the Hirshfeld surfaces were mapped using Crystal Explorer 21.5 v software [52,53]. The surface areas mapped with the shape-index (Figure 5) and the electrostatic potential (Figure 6) functions for the complex revealed close contacts between the phenolic ring and the metal chelate. The blue bump shape belongs to the donor, and the red hollowed spots correspond to the acceptor in an intermolecular interaction.

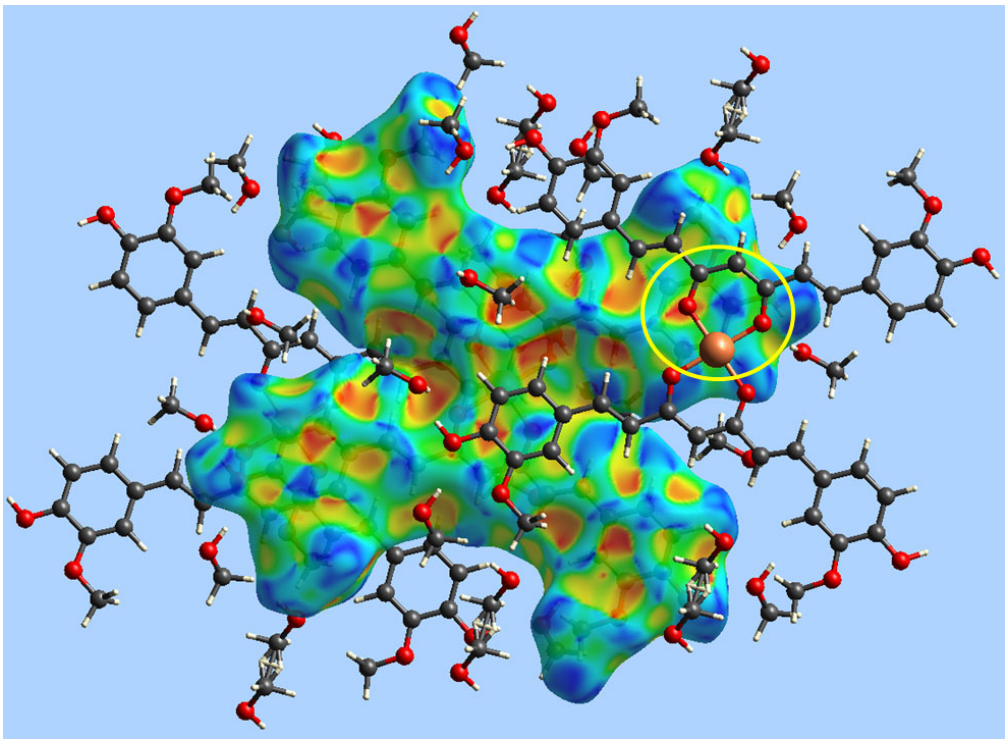

Figure 5. A view of the Hirshfeld surface mapped with the shape-index property illustrating the aromatic···metal chelate interaction (yellow circle).

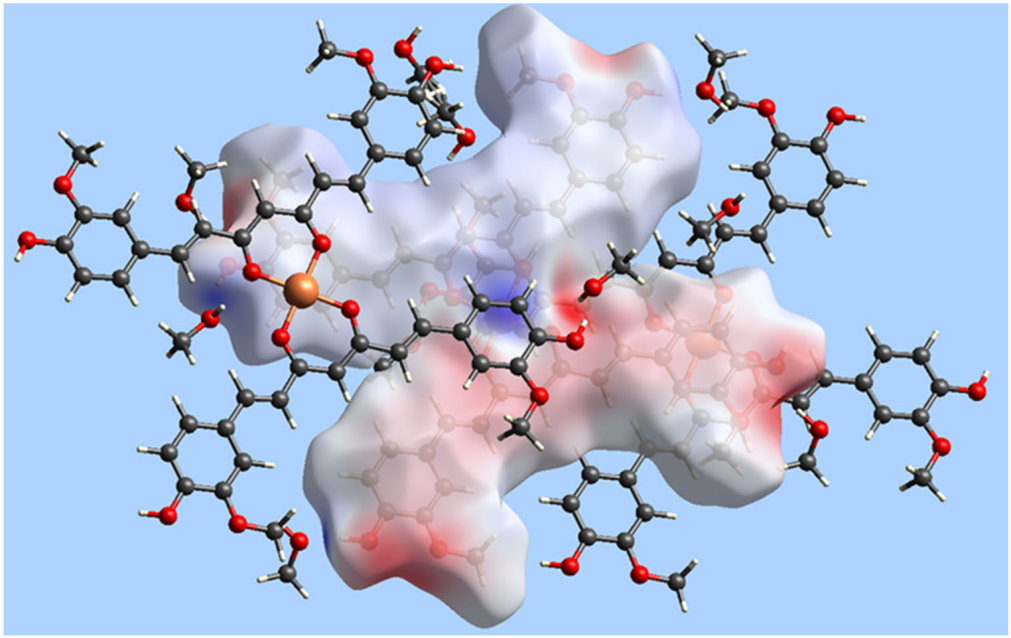

Figure 6. A view of the Hirshfeld surface for complex **1** mapped over the calculated electrostatic potential in the range −0.1178 to +0.2313 atomic units (the red and blue regions represent negative and positive electrostatic potentials, respectively).

The surface area was determined by the d_{norm} function for complex **1**, revealing close contacts (red regions) on the phenolic and methoxy groups (Figure 7). However, the 2D fingerprint plot shows the characteristic two peaks corresponding to O···H/H···O contacts (Figure 8a). Also, the greater percentage of contacts originate from H/H interactions followed by O···H/H···O contacts with 44.2 and 24.5 percent, respectively (Figure 8b).

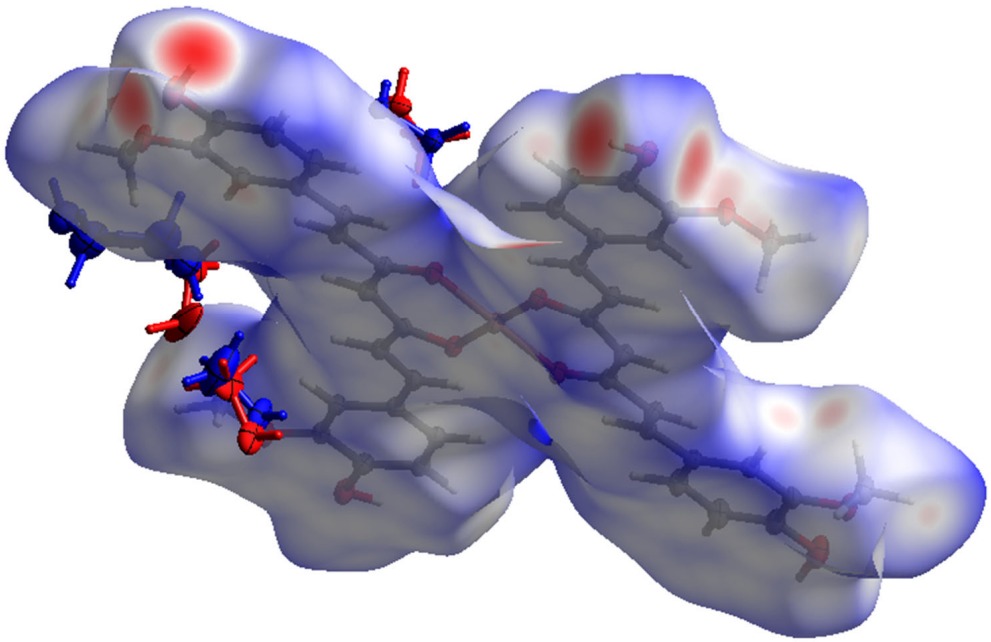

Figure 7. Hirshfeld surface (d_{norm}) of complex **1**. Molecules of disordered methanol are represented in red and blue ellipsoids.

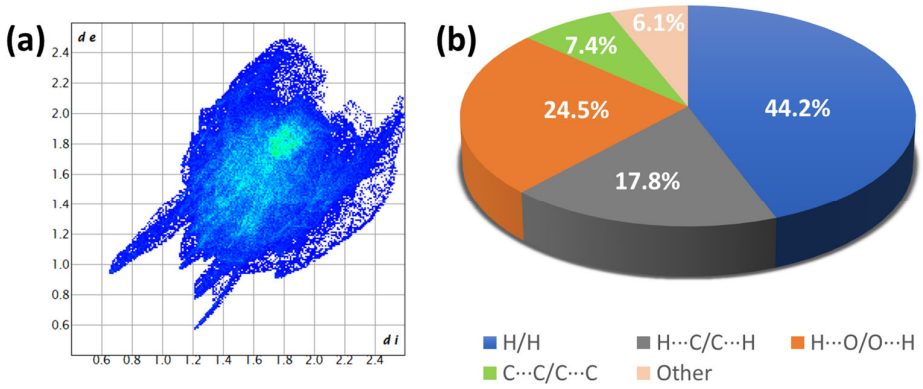

Figure 8. (**a**) Fingerprint plot of complex **1** from HS and (**b**) an individual percentage of contacts.

A survey for curcumin transition metal complexes on the Cambridge Structural Database, CSD version 5.42 updates (April 2023) [54] shows 23 structures where all of them contain just 1 molecule of curcumin as a ligand. Of these 23 structures, 8 [55–62] (CSD refcodes: PIRVET, HUKGEC, GEGLAH, FEGCOL, BUBSOJ (two molecules), DEYLUR, DOQWUE, GESYAG) display the *anti*, *s-cis*, *s-trans*, *anti*-conformation for the ligand. A comparison among this subset, including the curcumin ligand (QUMDIN) and complex **1**, was performed using the program CrystalCMP [63]. On the calculation of the differences in interatomic distances and the similarity is calculated as a positional difference between molecules in a representative molecular cluster. A very good agreement was found between the structure of ligand in Complex **1** and the corresponding structures found in the subset. A lesser agreement was observed for the pure ligand structure and that found in the complexes (Figure 9).

	0	1	2	3	4	5	6	7	8	9	10	label
0	0.000	1.164	1.103	1.179	1.377	1.436	1.131	1.537	1.554	1.555	0.513	0: 0QUMDIN.CURCUMIN.cif
1	1.164	0.000	0.049	0.088	0.089	0.105	0.111	0.091	0.402	0.418	0.639	1: 1Compound_1.cif
2	1.103	0.049	0.000	0.071	0.221	0.037	0.080	0.167	0.413	0.356	0.511	2: 2PIRVET.AntiAnti.cif
3	1.179	0.088	0.071	0.000	0.150	0.092	0.031	0.145	0.407	0.606	0.617	3: 3HUKGEC.AntiAnti.cif
4	1.377	0.089	0.221	0.150	0.000	0.240	0.169	0.127	0.224	0.202	0.671	4: 4GEGLAH.AntiAnti.cif
5	1.436	0.105	0.037	0.092	0.240	0.000	0.095	0.136	0.291	0.241	0.628	5: 5FEGCOL.AntiAnti.cif
6	1.131	0.111	0.080	0.031	0.169	0.095	0.000	0.280	0.790	0.686	0.589	6: 6BUBSOJ.AntiAnti.cif
7	1.537	0.091	0.167	0.145	0.127	0.136	0.280	0.000	0.408	0.415	0.753	7: 6BUBSOJ.AntiAnti.cif
8	1.554	0.402	0.413	0.407	0.224	0.291	0.790	0.408	0.000	0.047	0.624	8: 6DEYLUR.AntiAnti.cif
9	1.555	0.418	0.356	0.606	0.202	0.241	0.686	0.415	0.047	0.000	0.631	9: 7DOQWUE.AntiAnti.cif
10	0.513	0.639	0.511	0.617	0.671	0.628	0.589	0.753	0.624	0.631	0.000	10: 8GESYAG.AntiAnti.cif

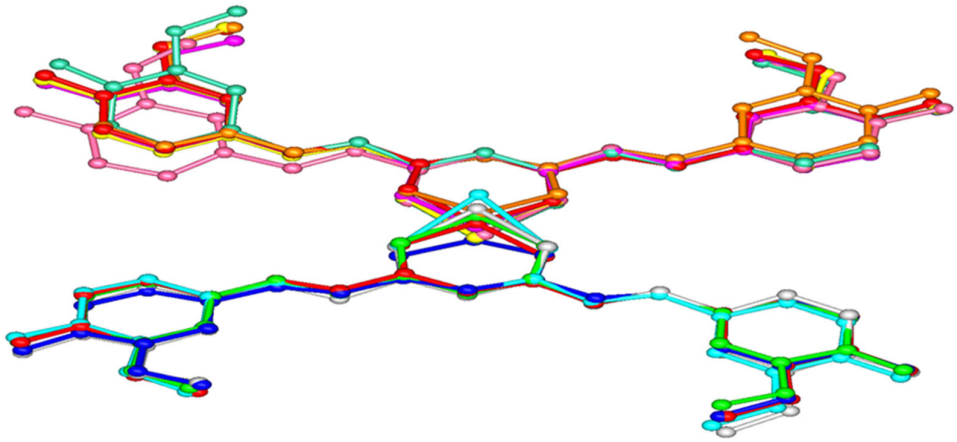

Figure 9. Similarity matrix (**top**) displaying the Root-Mean-Square-Deviation (RMSD) among the crystal structures compared and graphical overlay of these structures (**bottom**). Colors of the crystal structures correspond to the colors used in the second row of the similarity matrix.

Complex **1** was four times more active against the U-251 cell line (see Table 3) than the ligand (curcumin), which agrees with previous reports [64] and suggests that: (a) curcumin and the metal ion are mutually stabilized in the complex [27,65,66], (b) solubility and bioavailability are improved [67], and (c) the subsequent cell death occurs as a consequence of intercalation with DNA [68].

Table 3. Cytotoxic activity of complex **1** and curcumin.

Complex	U-251 (IC_{50} = μM)	K562 (IC_{50} = μM)
Complex (1)	5.2 ± 0.2	9.5 ± 0.3
Curcumin *	20.5 ± 1.7	16.4 ± 0.04

* Taken from the reference [69].

The log *p* value of curcumin is 3.1 ± 0.04, consistent with previous reports [70,71], while the log *p* of complex **1** was 2.3 ± 0.15, indicating that the latter has better water solubility and therefore better bioavailability.

The antioxidant assay (TBARS) of the copper–complex (**1**) showed enhanced activity with respect to the ligand (almost 3 times, see Table 4) and practically equaled that of BHT (Butylated hydroxytoluene), demonstrating that the copper within the complex plays an important role in the inhibition levels of malondialdehyde (MDA). Also, it is known that the curcumin–Cu^{+2} complex enhances the activities of several antioxidant enzymes (catalase, superoxide dismutase, and glutathione peroxidase) and attenuates the rise of MDA levels [72,73].

Table 4. Antioxidant activity of complex **1** and curcumin.

Complex	(IC_{50} = μM)
Complex (**1**)	1.24 ± 0.08
Curcumin	3.03 ± 0.15
BHT	1.22 ± 0.44

There is a concrete benefit in knowing the precise molecular structure from the X-rays determination of the single crystal of curcumin with copper since it will help to solve structural unknowns (geometry or metal-ligand relationship), as well as to explain different biological effects found, i.e., the antioxidant capacity of the complex, the high cytotoxic potential against cancer cells, and the potential of copper curcumin complex to combat Alzheimer's disease. Furthermore, it will support studies and scope in computational chemistry (QSAR, DFT, molecular docking, etc.).

4. Materials and Methods

Anhydrous copper (II) acetate was available commercially and purchased from Sigma-Aldrich. Pure curcumin was obtained from synthesis as previously reported [74]. The solvents were HPLC grade from Sigma-Aldrich.

4.1. Physical Measurements

The melting points were determined on an Electrothermal Engineering IA9100 × 1 melting point apparatus and are uncorrected.

4.2. Spectroscopic Determinations

The IR-ATR absorption spectra were recorded in the 4000–400 cm^{-1} range on a FT-IR NICOLET IS-50, Thermo Fisher Scientific spectrophotometer. The EPR spectra were recorded in DMSO at liquid nitrogen temperature (77 K) on an Electron Paramagnetic Resonance Spectrometer JEOL, JES-TE300, ITC Cryogenic System, Oxford. Mass spectra were recorded in a Bruker Esquire 6000 with electrospray, atmospheric pressure chemical ionization, and ion trap (ESI-TI). Uv-Vis was recorded on UV-VIS SHIMADZU 1800.

CP/MASS ^{13}C NMR spectra were recorded on a Jeol 600 MHz spectrometer (15.0 kHz of MAS) using adamantane as the reference (298 K).

4.3. Biological Assays

The cytotoxicity of curcumin and curcumin–copper complex **1** was tested against 6 cancer cell lines: U251 (human glioblastoma cell line), PC-3 (human Caucasian prostate adenocarcinoma), K562 (human Caucasian chronic myelogenous leukaemia), HCT-15 (human colon adenocarcinoma), MCF-7 (human mammary adenocarcinoma), and SKLU-1 (human lung adenocarcinoma). The cell viability in the experiments exceeded 95%, as determined with trypan blue. The human tumor cytotoxicity was determined using the protein-binding dye sulforhodamine B (SRB) in a microculture assay to measure cell growth, as described in the protocols established by the NCI and previously [69]. A dose–response curve was plotted for each complex and the concentration (IC_{50}), resulting in an inhibition of 50% estimated through non-linear regression analysis. Results were expressed as inhibitory concentration 50 (IC_{50}) values.

Antioxidant activity of curcumin and curcumin–copper complex were tested by Thiobarbituric Acid Reactive Substances (TBARS) method and were measured using rat brain homogenates according to the method described by Ng and co-workers [75], with some modifications as previously was recorded [76]. The concentration of TBARS was calculated by interpolation on a standard curve of tetra-methoxypropane (TMP) as a precursor of MDA [77]. Results are expressed as n moles of TBARS per mg of protein. The inhibition ratio (IR [%]) was calculated using the formula IR = (C–E) × 100/C, where C is the control absorbance and E is the sample absorbance. Butylated hydroxytoluene (BHT) was used as a positive standard. All data are presented as mean ± standard error (SEM). Data were analyzed by one-way analysis of variance (ANOVA) followed by Dunnett's test for comparison against control. Values of $p \leq 0.05$ (*) and $p \leq 0.01$ (**) were considered statistically significant.

4.4. Determination of Partition Coefficients

Partition coefficients were measured according to the shake–flask method previously reported [78,79], and the quantitation of the curcumin (8 μM) and Complex **1** (4 μM) was recorded by ultraviolet (UV) spectrophotometry. The experiments were conducted in triplicate and standard curves are found in the Supplementary Materials (Figures S18 and S19).

4.5. Synthesis of Complex **1**

In a 100 mL ball flask with 30 mL of methanol-HPLC, 200 mg of curcumin (0.54 mmol) was added and heated, and a methanolic (50 mL) solution containing 50 mg of anhydrous copper (II) acetate (0.27 mmol) was added dropwise. The reaction mixture was refluxed for 12 h. The volume was reduced to approximately 20 mL and the suspension was filtered off in a Hirsch funnel; the solid retained in the filter was washed with cold methanol water (8:2 *v*/*v*) and was left to stand at *vacuum* and room temperature for 4 hours. Solid phase: Amorphous solid, dark brown color, Yield= 20%. Melting point: 290–292 °C. MS (ESI^+) = 797.0 *m*/*z* $[M]^+$, 900.9 *m*/*z*. IR-ATR 3441 (O-H, phenol), 2999-2833 (C-H_{Ar}) 1619 (C=O), 1587 (C=C), 1491 (C=O-Cu), 965 (C–O, β-diketone), and 469 cm^{-1} (O-Cu).

The filtrate was slowly evaporated, rendering crystals that were filtered off in a Hirsch funnel and washed with cold methanol water (8:2 *v*/*v*). Crystals were left to stand in a *vacuum* at room temperature for four hours. Crystals, bright brown color, Yield= 50%. Melting point: 230 °C (decomposition). MS (ESI^+) = 820.0 *m*/*z* $[M + Na]^+$, 898.0 *m*/*z* $[[M + Na + DMSO]^+$. IR-ATR 3587 (O-H, MeOH), 3443 (O-H, phenol), 3039-3837 (C-H_{Ar}), 1621 (C=O), 1587 (C=C), 1496 (C=O-Cu), 963 (C–O, β-diketone), and 478 cm^{-1} (O-Cu). Elemental Analysis: Calculated for $C_{42}H_{38}CuO_{12}{\cdot}0.5H_2O$: C 62.49; H 4.87; experimental: C 62.32; H 4.80.

Single crystals formation (suitable for X-ray diffraction): 30 mg of crystals described previously were dissolved in 30 mL of anhydrous methanol-HPLC and filtered for elimina-

tion of solid impurities, this solution afforded crystals after slow evaporation for one week at room temperature.

4.6. Powder and Single-Crystal X-ray Diffraction Analysis

Powder X-ray diffraction (PXRD) was performed in the transmission mode on a BRUKER D8 ADVANCE diffractometer, under Cu Kα radiation (λ = 1.54059 Å). The equipment was operated at 40 kV and 40 mA, and data were collected at room temperature in the range of 2θ = 3–70°. PXRD data analyses were conducted using WinPLOTR [80].

Single-crystal X-ray diffraction studies for complex **1** were carried out on a Rigaku Xcalibur and Gemini with MoKα radiation (λ = 0.71073 Å) by performing ω scans frames at 130 K. Absorption correction was carried out empirically using SCALE3 ABSPACK scaling algorithm (CrysAlisPro, Agilent Technologies, Version 1.171.36.32 [81]) and refined by full-matrix least-squares treatment against $|F|2$ in anisotropic approximation with SHELXL-2019/3 [82] in the ShelXle program [83]. H-atoms were included in the geometrically calculated positions. Visualization and analysis of crystal structures were carried out using Mercury 2021.3.0 v [84] software.

5. Conclusions

We have successfully achieved the synthesis and the complete structure elucidation of the homoleptic ML_2 curcumin–copper complex, authenticated through single crystal X-ray diffraction, unequivocally demonstrating the 2:1 curcumin–metal ratio. An outstanding feature is that no substitution of the phenolic groups was necessary.

The supramolecular analysis demonstrates that the solvent plays a critical role in crystallization. Furthermore, the mother liquor (filtrate) should be considered a suitable source of crystals and not be underestimated. The supramolecular interactions in both amorphous and crystal phases are specific and different, with the solvent of crystallization playing a critical role. These subtle differences may be the key factor that has prevented the crystallization of pristine curcumin with a single-atom metal in the past.

The biological activity of the homoleptic curcumin–metal complex shows a dramatic increase in cytotoxicity and antioxidant properties compared to pristine curcumin. Therefore, the search for other homoleptic crystal structures of curcumin with different metals is a task to be undertaken in the short future.

Therapeutic areas such as Alzheimer's disease, degenerative neurological ailments, and cancer research, and the search for antioxidant agents may hopefully expand their scope from the present finding.

Supplementary Materials: The following supporting information can be downloaded at: https://www.mdpi.com/article/10.3390/molecules28166033/s1, Figure S1: The molecular structure of complex **1** including molecules of solvent (methanol) and the disordered position of methanol (green ellipsoids). Figure S2: Mass spectrum of complex **1** (dark brown solid) by ESI^+ previously dissolved in DMSO. Figure S3: Mass spectrum of complex **1** (brilliant brown solid) by ESI^+ previously dissolved in DMSO. Figure S4: Amplification of Mass spectrum of complex **1** (brilliant brown solid) by ESI^+ previously dissolved in DMSO. Figure S5: Grow process of a monocrystal of complex **1**: (a) Recrystallization of the filtrate and filtration in a Hirsch funnel, (b) amplified view of crystals, and (c) Monocrystals obtained after slow evaporation in methanol. Figure S6: Solid state Electron Paramagnetic Resonance of amorphous material (dark brown solid). Figure S7: ^{13}C CP/MAS spectrum of curcumin. Figure S8: ^{13}C CP/MASS spectrum of complex (**1**). Figure S9: IR-ATR spectrum of free curcumin. Figure S10: IR-ATR spectrum of complex (**1**) dark brown solid. Figure S11: IR-ATR spectrum of complex (1) brilliant brown crystalline solid. Figure S12: UV-Vis spectrum of complex (**1**) dark brown solid (REF: Methanol, Max = 422nm). Figure S13: UV-Vis spectra of complex (**1**) brilliant brown crystalline solid (REF: Methanol, Max = 421 nm) and free curcumin (REF: Methanol, Max = 420 nm). Figure S14: Powder XRD pattern of complex **1** (bright brown material). Figure S15: Powder XRD pattern of complex **1** (amorphous solid). Figure S16: Comparison of PXRD patterns of complex **1** (red: simulated, 130K); blue: crystalline material; gold: amorphous material). Figure S17: Inhibition curve of Lipid Peroxidation on Rat Brain. Figure S18: Adj. R-Square of Cur-

cumin in 1-Octanol. Figure S19: Adj. R-Square of Complex **1** in 1-Octanol. Table S1: Crystallographic data of complex **1**. Table S2: Growth inhibition percentages of cancerous and noncancerous (COS-7) cell lines by compounds (9.9 μM, 48 h). Table S3: Inhibition of Lipid Peroxidation on Rat Brain. CCDC 2271944 contain the supplementary crystallographic data for this paper. These data can be obtained free of charge via www.ccdc.cam.ac.uk/cgi-bin/catreq.cgi (accessed on 27 June 2023), by e-mailing data_request@ccdc.cam.ac.uk, or by contacting: The Cambridge Crystallographic Data Centre, 12 Union Road, Cambridge CB2 1EZ, UK, Fax; +44(0)-1223-336033.

Author Contributions: A.A.-C.: Investigation, Formal analysis, Writing—original draft, Writing—review and editing. M.A.O.-M.: Investigation, Formal analysis, Writing—original draft, Writing—review and editing. W.M.-M.: Investigation, Formal analysis. M.T.R.-A.: Investigation, Formal analysis. A.N.-C.: Investigation, Formal analysis. R.A.T.: Investigation, Validation, Formal analysis. R.S.-O.: Investigation, Formal analysis, Writing—original draft. L.L.P.-G.: Investigation. R.G.E.: Conceptualization, Methodology, Formal analysis, Validation, Writing—original draft, Writing—review and editing, Visualization, Supervision, Project administration, Funding acquisition. All authors have read and agreed to the published version of the manuscript.

Funding: This research was funded by CONAHCyT FOINS-307152 and DGAPA PAPIIT-IT200720.

Institutional Review Board Statement: Not applicable.

Informed Consent Statement: Not applicable.

Data Availability Statement: Not applicable.

Acknowledgments: A.A.-C. is grateful to CONAHCyT for the postdoctoral fellowship (CVU: 565984). R.G.E. thanks for the financing of CONAHCyT FOINS-307152 and DGAPA PAPIIT-IT200720. M.A.O.-M. thanks for the payment of project fees CONAHCyT FOINS-307152. L.L.P.-G. is grateful to CONAHCyT (CVU: 1234478). We are indebted to María de la Paz Orta Perez (AE), Adriana Romo (IR), Virginia Gómez Vidales (EPR), and Lucero Rios Ruiz (ESI) from Instituto de Química, UNAM, QI. María Cecilia Salcedo, Rosa Isela del Villar Morales, Facultad de Química-UNAM, USAII for X-ray data collection and CPMAS. MVZ Claudia V. Rivera Cerecedo and MVZ Héctor Malagón Rivero from Bioterio de Fisiología Celular (UNAM) for providing the rat brain.

Conflicts of Interest: The authors declare no conflict of interest.

Sample Availability: A sample of complex **1** is available from the authors.

References

1. Hewlings, S.J.; Kalman, D.S. Curcumin: A Review of Its Effects on Human Health. *Foods* **2017**, *6*, 92. [CrossRef] [PubMed]
2. Prasad, S.; Dubourdieu, D.; Srivastava, A.; Kumar, P.; Lall, R. Metal–Curcumin Complexes in Therapeutics: An Approach to Enhance Pharmacological Effects of Curcumin. *Int. J. Mol. Sci.* **2021**, *22*, 7094. [CrossRef] [PubMed]
3. Mishra, S.; Palanivelu, K. The Effect of Curcumin (Turmeric) on Alzheimer's Disease: An Overview. *Ann. Indian. Acad. Neurol.* **2008**, *11*, 13. [CrossRef]
4. Boarescu, P.M.; Boarescu, I.; Bocșan, I.C.; Gheban, D.; Bulboacă, A.E.; Nicula, C.; Pop, R.M.; Râjnoveanu, R.M.; Bolboacă, S.D. Antioxidant and Anti-Inflammatory Effects of Curcumin Nanoparticles on Drug-Induced Acute Myocardial Infarction in Diabetic Rats. *Antioxidants* **2019**, *8*, 504. [CrossRef] [PubMed]
5. Hussain, H.; Ahmad, S.; Shah, S.W.A.; Ullah, A.; Rahman, S.U.; Ahmad, M.; Almehmadi, M.; Abdulaziz, O.; Allahyani, M.; Alsaiari, A.A.; et al. Synthetic Mono-Carbonyl Curcumin Analogues Attenuate Oxidative Stress in Mouse Models. *Biomedicines* **2022**, *10*, 2597. [CrossRef]
6. Witika, B.A.; Makoni, P.A.; Matafwali, S.K.; Mweetwa, L.L.; Shandele, G.C.; Walker, R.B. Enhancement of Biological and Pharmacological Properties of an Encapsulated Polyphenol: Curcumin. *Molecules* **2021**, *26*, 4244. [CrossRef]
7. Ghosh, S.; Banerjee, S.; Sil, P.C. The Beneficial Role of Curcumin on Inflammation, Diabetes and Neurodegenerative Disease: A Recent Update. *Food Chem. Toxicol.* **2015**, *83*, 111–124. [CrossRef]
8. Chauhan, G.; Rath, G.; Goyal, A.K. In-Vitro Anti-Viral Screening and Cytotoxicity Evaluation of Copper-Curcumin Complex. *Artif. Cells Nanomed. Biotechnol.* **2013**, *41*, 276–281. [CrossRef]
9. Reddy, R.C.; Vatsala, P.G.; Keshamouni, V.G.; Padmanaban, G.; Rangarajan, P.N. Curcumin for Malaria Therapy. *Biochem. Biophys. Res. Commun.* **2005**, *326*, 472–474. [CrossRef]
10. Mahady, G.B.; Pendland, S.L.; Yun, G.; Lu, Z.Z. Turmeric (Curcuma Longa) and Curcumin Inhibit the Growth of Helicobacter Pylori, a Group 1 Carcinogen. *Anticancer Res.* **2002**, *22*, 4179–4181. [PubMed]
11. Ghorbani, Z.; Hekmatdoost, A.; Mirmiran, P. Anti-Hyperglycemic and Insulin Sensitizer Effects of Turmeric and Its Principle Constituent Curcumin. *Int. J. Endocrinol. Metab.* **2014**, *12*, e18081. [CrossRef]

12. Quispe, C.; Herrera-Bravo, J.; Javed, Z.; Khan, K.; Raza, S.; Gulsunoglu-Konuskan, Z.; Daştan, S.D.; Sytar, O.; Martorell, M.; Sharifi-Rad, J.; et al. Therapeutic Applications of Curcumin in Diabetes: A Review and Perspective. *BioMed Res. Int.* **2022**, *2022*, 1375892. [CrossRef] [PubMed]
13. Lei, F.; Li, P.; Chen, T.; Wang, Q.; Wang, C.; Liu, Y.; Deng, Y.; Zhang, Z.; Xu, M.; Tian, J.; et al. Recent Advances in Curcumin-Loaded Biomimetic Nanomedicines for Targeted Therapies. *J. Drug Deliv. Sci. Technol.* **2023**, *80*, 104200. [CrossRef]
14. de Waure, C.; Bertola, C.; Baccarini, G.; Chiavarini, M.; Mancuso, C. Exploring the Contribution of Curcumin to Cancer Therapy: A Systematic Review of Randomized Controlled Trials. *Pharmaceutics* **2023**, *15*, 1275. [CrossRef] [PubMed]
15. Kong, W.-Y.; Ngai, S.C.; Goh, B.-H.; Lee, L.-H.; Htar, T.-T.; Chuah, L.-H. Is Curcumin the Answer to Future Chemotherapy Cocktail? *Molecules* **2021**, *26*, 4329. [CrossRef]
16. Zoi, V.; Galani, V.; Lianos, G.D.; Voulgaris, S.; Kyritsis, A.P.; Alexiou, G.A. The Role of Curcumin in Cancer Treatment. *Biomedicines* **2021**, *9*, 1086. [CrossRef]
17. Jalili-Nik, M.; Soltani, A.; Moussavi, S.; Ghayour-Mobarhan, M.; Ferns, G.A.; Hassanian, S.M.; Avan, A. Current Status and Future Prospective of Curcumin as a Potential Therapeutic Agent in the Treatment of Colorectal Cancer. *J. Cell Physiol.* **2018**, *233*, 6337–6345. [CrossRef]
18. Devassy, J.G.; Nwachukwu, I.D.; Jones, P.J.H. Curcumin and Cancer: Barriers to Obtaining a Health Claim. *Nutr. Rev.* **2015**, *73*, 155–165. [CrossRef]
19. Ravindran, J.; Prasad, S.; Aggarwal, B.B. Curcumin and Cancer Cells: How Many Ways Can Curry Kill Tumor Cells Selectively? *AAPS J.* **2009**, *11*, 495–510. [CrossRef]
20. Anand, P.; Kunnumakkara, A.B.; Newman, R.A.; Aggarwal, B.B. Bioavailability of Curcumin: Problems and Promises. *Mol. Pharm.* **2007**, *4*, 807–818. [CrossRef]
21. Prasad, S.; Tyagi, A.K.; Aggarwal, B.B. Recent Developments in Delivery, Bioavailability, Absorption and Metabolism of Curcumin: The Golden Pigment from Golden Spice. *Cancer Res. Treat.* **2014**, *46*, 2–18. [CrossRef] [PubMed]
22. Sohn, S.-I.; Priya, A.; Balasubramaniam, B.; Muthuramalingam, P.; Sivasankar, C.; Selvaraj, A.; Valliammai, A.; Jothi, R.; Pandian, S. Biomedical Applications and Bioavailability of Curcumin—An Updated Overview. *Pharmaceutics* **2021**, *13*, 2102. [CrossRef] [PubMed]
23. Shen, L.; Ji, H.-F. The Pharmacology of Curcumin: Is It the Degradation Products? *Trends Mol. Med.* **2012**, *18*, 138–144. [CrossRef] [PubMed]
24. Wang, J.; Wei, D.; Jiang, B.; Liu, T.; Ni, J.; Zhou, S. Two Copper(II) Complexes of Curcumin Derivatives: Synthesis, Crystal Structure and in Vitro Antitumor Activity. *Transit. Metal Chem.* **2014**, *39*, 553–558. [CrossRef]
25. Basile, V.; Ferrari, E.; Lazzari, S.; Belluti, S.; Pignedoli, F.; Imbriano, C. Curcumin Derivatives: Molecular Basis of Their Anti-Cancer Activity. *Biochem. Pharmacol.* **2009**, *78*, 1305–1315. [CrossRef]
26. Medigue, N.E.H.; Bouakouk-Chitti, Z.; Bechohra, L.L.; Kellou-Taïri, S. Theoretical Study of the Impact of Metal Complexation on the Reactivity Properties of Curcumin and Its Diacetylated Derivative as Antioxidant Agents. *J. Mol. Model.* **2021**, *27*, 192. [CrossRef]
27. Wanninger, S.; Lorenz, V.; Subhan, A.; Edelmann, F.T. Metal Complexes of Curcumin—Synthetic Strategies, Structures and Medicinal Applications. *Chem. Soc. Rev.* **2015**, *44*, 4986–5002. [CrossRef]
28. Barik, A.; Mishra, B.; Kunwar, A.; Kadam, R.M.; Shen, L.; Dutta, S.; Padhye, S.; Satpati, A.K.; Zhang, H.Y.; Indira Priyadarsini, K. Comparative Study of Copper(II)-Curcumin Complexes as Superoxide Dismutase Mimics and Free Radical Scavengers. *Eur. J. Med. Chem.* **2007**, *42*, 431–439. [CrossRef]
29. Leung Mandy, H.M.; Harada, T.; Kee Tak, W. Delivery of Curcumin and Medicinal Effects of the Copper(II)-Curcumin Complexes. *Curr. Pharm. Des.* **2013**, *19*, 2070–2083. [CrossRef]
30. Vajragupta, O. Manganese Complexes of Curcumin and Its Derivatives: Evaluation for the Radical Scavenging Ability and Neuroprotective Activity. *Free Radic. Biol. Med.* **2003**, *35*, 1632–1644. [CrossRef]
31. Khalil, M.I.; Al-Zahem, A.M.; Al-Qunaibit, M.H. Synthesis, Characterization, Mössbauer Parameters, and Antitumor Activity of Fe(III) Curcumin Complex. *Bioinorg. Chem. Appl.* **2013**, *2013*, 982423. [CrossRef] [PubMed]
32. Al-Noor, T.H.; Ali, A.M.; Al-Sarray, A.J.A.; Al-Obaidi, O.H.; Obeidat, A.I.M.; Habash, R.R. A Short Review: Chemistry of Curcumin and Its Metal Complex Derivatives. *J. Univ. Anbar Pure Sci.* **2022**, *16*, 20–26. [CrossRef]
33. Portolés-Gil, N.; Lanza, A.; Aliaga-Alcalde, N.; Ayllón, J.A.; Gemmi, M.; Mugnaioli, E.; López-Periago, A.M.; Domingo, C. Crystalline Curcumin BioMOF Obtained by Precipitation in Supercritical CO_2 and Structural Determination by Electron Diffraction Tomography. *ACS Sustain. Chem. Eng.* **2018**, *6*, 12309–12319. [CrossRef]
34. Su, H.; Sun, F.; Jia, J.; He, H.; Wang, A.; Zhu, G. A Highly Porous Medical Metal–Organic Framework Constructed from Bioactive Curcumin. *Chem. Commun.* **2015**, *51*, 5774–5777. [CrossRef] [PubMed]
35. Wazir, S.M.; Ghobrial, I. Copper Deficiency, a New Triad: Anemia, Leucopenia, and Myeloneuropathy. *J. Community Hosp. Intern. Med. Perspect.* **2017**, *7*, 265–268. [CrossRef]
36. Sierpinska, T.; Konstantynowicz, J.; Orywal, K.; Golebiewska, M.; Szmitkowski, M. Copper Deficit as a Potential Pathogenic Factor of Reduced Bone Mineral Density and Severe Tooth Wear. *Osteoporos. Int.* **2014**, *25*, 447–454. [CrossRef]
37. Percival, S. Copper and Immunity. *Am. J. Clin. Nutr.* **1998**, *67*, 1064S–1068S. [CrossRef]
38. Collins, J.F.; Klevay, L.M. Copper. *Adv. Nutr.* **2011**, *2*, 520–522. [CrossRef]
39. Desai, V.; Kaler, S.G. Role of Copper in Human Neurological Disorders. *Am. J. Clin. Nutr.* **2008**, *88*, 855S–858S. [CrossRef]

40. Xu, G.; Wang, J.; Liu, T.; Wang, M.; Zhou, S.; Wu, B.; Jiang, M. Synthesis and Crystal Structure of a Novel Copper(II) Complex of Curcumin-Type and Its Application in in Vitro and in Vivo Imaging. *J. Mater. Chem. B* **2014**, *2*, 3659–3666. [CrossRef] [PubMed]
41. Pi, Z.; Wang, J.; Jiang, B.; Cheng, G.; Zhou, S. A Curcumin-Based TPA Four-Branched Copper(II) Complex Probe for in Vivo Early Tumor Detection. *Mater. Sci. Eng. C* **2015**, *46*, 565–571. [CrossRef] [PubMed]
42. Zhang, W.; Chen, C.; Shi, H.; Yang, M.; Liu, Y.; Ji, P.; Chen, H.; Tan, R.X.; Li, E. Curcumin Is a Biologically Active Copper Chelator with Antitumor Activity. *Phytomedicine* **2016**, *23*, 1–8. [CrossRef] [PubMed]
43. Angulo, J.; Delgado-Villanueva, J. Preparación y Caracterización de Complejos de Curcumina Con Zinc(II), Níquel(II), Magnesio(II), Cobre(II) y Su Evaluación Frente a Bacterias Grampositiva y Gramnegativa. *Rev. Politécnica* **2023**, *51*, 63–72. [CrossRef]
44. Su, H.; He, H.; Tian, Y.; Zhao, N.; Sun, F.; Zhang, X.; Jiang, Q.; Zhu, G. Syntheses and Characterizations of Two Curcumin-Based Cocrystals. *Inorg. Chem. Commun.* **2015**, *55*, 92–95. [CrossRef]
45. Matlinska, M.A.; Wasylishen, R.E.; Bernard, G.M.; Terskikh, V.V.; Brinkmann, A.; Michaelis, V.K. Capturing Elusive Polymorphs of Curcumin: A Structural Characterization and Computational Study. *Cryst. Growth Des.* **2018**, *18*, 5556–5563. [CrossRef]
46. Rajesh, J.; Gubendran, A.; Rajagopal, G.; Athappan, P. Synthesis, Spectra and DNA Interactions of Certain Mononuclear Transition Metal(II) Complexes of Macrocyclic Tetraaza Diacetyl Curcumin Ligand. *J. Mol. Struct.* **2012**, *1010*, 169–178. [CrossRef]
47. Barik, A.; Mishra, B.; Shen, L.; Mohan, H.; Kadam, R.M.; Dutta, S.; Zhang, H.-Y.; Priyadarsini, K.I. Evaluation of a New Copper(II)–Curcumin Complex as Superoxide Dismutase Mimic and Its Free Radical Reactions. *Free Radic. Biol. Med.* **2005**, *39*, 811–822. [CrossRef]
48. Sumi, M.; Nevaditha, N.T.; Sindhu Kumari, B. Synthesis, Spectroscopic Investigation and Bioactivities of Metal Complexes from Curcuma Longa Derivative. *Inorganica Chim. Acta* **2023**, *549*, 121397. [CrossRef]
49. Shakeel Nawaz, S.; Manjunatha, K.B.; Ranganatha, S.; Supriya, S.; Ramakrishna, D. Z-Scan and Degenerate Four Wave Mixing Studies on Newly Synthesized Copper Complexes of Curcumin. *Mater. Today Commun.* **2023**, *36*, 106601. [CrossRef]
50. Subhan, M.A.; Alam, K.; Rahaman, M.S.; Rahman, M.A.; Awal, R. Synthesis and Characterization of Metal Complexes Containing Curcumin ($C_{21}H_{20}O_6$) and Study of Their Anti-Microbial Activities and DNA-Binding Properties. *J. Sci. Res.* **2013**, *6*, 97–109. [CrossRef]
51. Leung, M.H.M.; Pham, D.-T.; Lincoln, S.F.; Kee, T.W. Femtosecond Transient Absorption Spectroscopy of Copper(Ii)–Curcumin Complexes. *Phys. Chem. Chem. Phys.* **2012**, *14*, 13580. [CrossRef]
52. McKinnon, J.J.; Jayatilaka, D.; Spackman, M.A. Towards Quantitative Analysis of Intermolecular Interactions with Hirshfeld Surfaces. *Chem. Commun.* **2007**, *37*, 3814–3816. [CrossRef] [PubMed]
53. Spackman, M.A.; McKinnon, J.J. Fingerprinting Intermolecular Interactions in Molecular Crystals. *CrystEngComm* **2002**, *4*, 378–392. [CrossRef]
54. Allen, F.H. The Cambridge Structural Database: A Quarter of a Million Crystal Structures and Rising. *Acta Crystallogr. B* **2002**, *58*, 380–388. [CrossRef] [PubMed]
55. Caruso, F.; Rossi, M.; Benson, A.; Opazo, C.; Freedman, D.; Monti, E.; Gariboldi, M.B.; Shaulky, J.; Marchetti, F.; Pettinari, R.; et al. Ruthenium-Arene Complexes of Curcumin: X-ray and Density Functional Theory Structure, Synthesis, and Spectroscopic Characterization, in Vitro Antitumor Activity, and DNA Docking Studies of (p-Cymene)Ru(Curcuminato)Chloro. *J. Med. Chem.* **2012**, *55*, 1072–1081. [CrossRef]
56. Pettinari, R.; Marchetti, F.; Di Nicola, C.; Pettinari, C.; Cuccioloni, M.; Bonfili, L.; Eleuteri, A.M.; Therrien, B.; Batchelor, L.K.; Dyson, P.J. Novel Osmium(II)–Cymene Complexes Containing Curcumin and Bisdemethoxycurcumin Ligands. *Inorg. Chem. Front.* **2019**, *6*, 2448–2457. [CrossRef]
57. Pettinari, R.; Petrini, A.; Marchetti, F.; Di Nicola, C.; Scopelliti, R.; Riedel, T.; Pittet, L.D.; Galindo, A.; Dyson., P.J. Influence of Functionalized η^6-Arene Rings on Ruthenium(II) Curcuminoids Complexes. *ChemistrySelect* **2018**, *3*, 6696–6700. [CrossRef]
58. da Silva, B.A.; Pitasse-Santos, P.; Sueth-Santiago, V.; Monteiro, A.R.M.; Marra, R.K.F.; Guedes, G.P.; Ribeiro, R.R.; de Lima, M.E.F.; Decoté-Ricardo, D.; Neves, A.P. Effects of Cu(II) and Zn(II) Coordination on the Trypanocidal Activities of Curcuminoid-Based Ligands. *Inorganica Chim. Acta* **2020**, *501*, 119237. [CrossRef]
59. Hussain, A.; Somyajit, K.; Banik, B.; Banerjee, S.; Nagaraju, G.; Chakravarty, A.R. Enhancing the Photocytotoxic Potential of Curcumin on Terpyridyl Lanthanide(III) Complex Formation. *Dalton Trans.* **2013**, *42*, 182–195. [CrossRef]
60. Banerjee, S.; Prasad, P.; Hussain, A.; Khan, I.; Kondaiah, P.; Chakravarty, A.R. Remarkable Photocytotoxicity of Curcumin in HeLa Cells in Visible Light and Arresting Its Degradation on Oxovanadium(Iv) Complex Formation. *Chem. Commun.* **2012**, *48*, 7702. [CrossRef]
61. Halevas, E.; Pekou, A.; Papi, R.; Mavroidi, B.; Hatzidimitriou, A.G.; Zahariou, G.; Litsardakis, G.; Sagnou, M.; Pelecanou, M.; Pantazaki, A.A. Synthesis, Physicochemical Characterization and Biological Properties of Two Novel Cu(II) Complexes Based on Natural Products Curcumin and Quercetin. *J. Inorg. Biochem.* **2020**, *208*, 111083. [CrossRef] [PubMed]
62. Triantis, C.; Tsotakos, T.; Tsoukalas, C.; Sagnou, M.; Raptopoulou, C.; Terzis, A.; Psycharis, V.; Pelecanou, M.; Pirmettis, I.; Papadopoulos, M. Synthesis and Characterization of *fac*-[$M(CO)_3(P)(OO)$] and *cis-trans*-[$M(CO)_2(P)_2(OO)$] Complexes (M = Re, ^{99m}Tc) with Acetylacetone and Curcumin as OO Donor Bidentate Ligands. *Inorg. Chem.* **2013**, *52*, 12995–13003. [CrossRef] [PubMed]
63. Rohlíček, J.; Skořepová, E.; Babor, M.; Čejka, J. *CrystalCMP*: An Easy-to-Use Tool for Fast Comparison of Molecular Packing. *J. Appl. Crystallogr.* **2016**, *49*, 2172–2183. [CrossRef]

64. Yan, F.-S.; Sun, J.-L.; Xie, W.-H.; Shen, L.; Ji, H.-F. Neuroprotective Effects and Mechanisms of Curcumin–Cu(II) and –Zn(II) Complexes Systems and Their Pharmacological Implications. *Nutrients* **2017**, *10*, 28. [CrossRef]
65. Zebib, B.; Mouloungui, Z.; Noirot, V. Stabilization of Curcumin by Complexation with Divalent Cations in Glycerol/Water System. *Bioinorg. Chem. Appl.* **2010**, *2010*, 292760. [CrossRef]
66. Khorasani, M.Y.; Langari, H.; Sany, S.B.T.; Rezayi, M.; Sahebkar, A. The Role of Curcumin and Its Derivatives in Sensory Applications. *Mater. Sci. Eng. C* **2019**, *103*, 109792. [CrossRef]
67. Shakeri, A.; Panahi, Y.; Johnston, T.P.; Sahebkar, A. Biological Properties of Metal Complexes of Curcumin. *BioFactors* **2019**, *45*, 304–317. [CrossRef]
68. Shahabadi, N.; Falsafi, M.; Moghadam, N.H. DNA Interaction Studies of a Novel Cu(II) Complex as an Intercalator Containing Curcumin and Bathophenanthroline Ligands. *J. Photochem. Photobiol. B* **2013**, *122*, 45–51. [CrossRef]
69. Meza-Morales, W.; Alvarez-Ricardo, Y.; Obregón-Mendoza, M.A.; Arenaza-Corona, A.; Ramírez-Apan, M.T.; Toscano, R.A.; Poveda-Jaramillo, J.C.; Enríquez, R.G. Three New Coordination Geometries of Homoleptic Zn Complexes of Curcuminoids and Their High Antiproliferative Potential. *RSC Adv.* **2023**, *13*, 8577–8585. [CrossRef]
70. Priyadarsini, K. The Chemistry of Curcumin: From Extraction to Therapeutic Agent. *Molecules* **2014**, *19*, 20091–20112. [CrossRef] [PubMed]
71. Bhaskar Rao, A.; Prasad, E.; Deepthi, S.S.; Ansari, I.A. Synthesis and Biological Evaluation of Glucosyl Curcuminoids. *Arch. Pharm.* **2014**, *347*, 834–839. [CrossRef] [PubMed]
72. Priya, R.S.; Balachandran, S.; Daisy, J.; Mohanan, P.V. Reactive Centers of Curcumin and the Possible Role of Metal Complexes of Curcumin as Antioxidants. *Univers. J. Phys. Appl.* **2015**, *9*, 6–16. [CrossRef]
73. Jakubczyk, K.; Drużga, A.; Katarzyna, J.; Skonieczna-Żydecka, K. Antioxidant Potential of Curcumin—A Meta-Analysis of Randomized Clinical Trials. *Antioxidants* **2020**, *9*, 1092. [CrossRef]
74. Obregón-Mendoza, M.A.; Meza-Morales, W.; Alvarez-Ricardo, Y.; Estévez-Carmona, M.M.; Enríquez, R.G. High Yield Synthesis of Curcumin and Symmetric Curcuminoids: A "Click" and "Unclick" Chemistry Approach. *Molecules* **2022**, *28*, 289. [CrossRef]
75. Ng, T.B.; Liu, F.; Wang, Z.T. Antioxidative Activity of Natural Products from Plants. *Life Sci.* **2000**, *66*, 709–723. [CrossRef] [PubMed]
76. Meza-Morales, W.; Alejo-Osorio, Y.; Alvarez-Ricardo, Y.; Obregón-Mendoza, M.A.; Machado-Rodriguez, J.C.; Arenaza-Corona, A.; Toscano, R.A.; Ramírez-Apan, M.T.; Enríquez, R.G. Homoleptic Complexes of Heterocyclic Curcuminoids with Mg(II) and Cu(II): First Conformationally Heteroleptic Case, Crystal Structures, and Biological Properties. *Molecules* **2023**, *28*, 1434. [CrossRef] [PubMed]
77. Ohkawa, H.; Ohishi, N.; Yagi, K. Assay for Lipid Peroxides in Animal Tissues by Thiobarbituric Acid Reaction. *Anal. Biochem.* **1979**, *95*, 351–358. [CrossRef]
78. Obregón-Mendoza, M.A.; Arias-Olguín, I.I.; Estévez-Carmona, M.M.; Meza-Morales, W.; Alvarez-Ricardo, Y.; Toscano, R.A.; Arenas-Huertero, F.; Cassani, J.; Enríquez, R.G. Non-Cytotoxic Dibenzyl and Difluoroborate Curcuminoid Fluorophores Allow Visualization of Nucleus or Cytoplasm in Bioimaging. *Molecules* **2020**, *25*, 3205. [CrossRef]
79. Andrés, A.; Rosés, M.; Ràfols, C.; Bosch, E.; Espinosa, S.; Segarra, V.; Huerta, J.M. Setup and Validation of Shake-Flask Procedures for the Determination of Partition Coefficients (LogD) from Low Drug Amounts. *Eur. J. Pharm. Sci.* **2015**, *76*, 181–191. [CrossRef]
80. Roisnel, T.; Rodriguez-Carvajal, J. WinPLOTR: A windows tool for powder diffraction patterns analysis materials science forum. In Proceedings of the Seventh European Powder Diffraction Conference (EPDIC 7), Barcelona, Spain, 20–23 May 2000; pp. 118–123.
81. Sheldrick, G.M. *SHELXT*—Integrated Space-Group and Crystal-Structure Determination. *Acta Crystallogr. A Found. Adv.* **2015**, *71*, 3–8. [CrossRef]
82. Sheldrick, G.M. Crystal Structure Refinement with *SHELXL*. *Acta Crystallogr. C Struct. Chem.* **2015**, *71*, 3–8. [CrossRef] [PubMed]
83. Hübschle, C.B.; Sheldrick, G.M.; Dittrich, B. *ShelXle*: A Qt Graphical User Interface for *SHELXL*. *J. Appl. Crystallogr.* **2011**, *44*, 1281–1284. [CrossRef] [PubMed]
84. Macrae, C.F.; Sovago, I.; Cottrell, S.J.; Galek, P.T.A.; McCabe, P.; Pidcock, E.; Platings, M.; Shields, G.P.; Stevens, J.S.; Towler, M.; et al. *Mercury 4.0*: From Visualization to Analysis, Design and Prediction. *J. Appl. Crystallogr.* **2020**, *53*, 226–235. [CrossRef] [PubMed]